Population of collective modes in light scattering by many atoms

William Guerin* and Robin Kaiser
Université Côte d'Azur, CNRS, Institut de Physique de Nice, France
(Received 1 February 2017; published 26 May 2017)

The interaction of light with an atomic sample containing a large number of particles gives rise to many collective (or cooperative) effects, such as multiple scattering, superradiance, and subradiance, even if the atomic density is low and the incident optical intensity weak (linear optics regime). Tracing over the degrees of freedom of the light field, the system can be well described by an effective atomic Hamiltonian, which contains the light-mediated dipole-dipole interaction between atoms. This long-range interaction is at the origin of the various collective effects, or of collective excitation modes of the system. Even though an analysis of the eigenvalues and eigenfunctions of these collective modes does allow distinguishing superradiant modes, for instance, from other collective modes, this is not sufficient to understand the dynamics of a driven system, as not all collective modes are significantly populated. Here, we study how the excitation parameters, i.e., the driving field, determines the population of the collective modes. We investigate in particular the role of the laser detuning from the atomic transition, and demonstrate a simple relation between the detuning and the steady-state population of the modes. This relation allows understanding several properties of cooperative scattering, such as why superradiance and subradiance become independent of the detuning at large enough detuning without vanishing, and why superradiance, but not subradiance, is suppressed near resonance. We also show that the spatial properties of the collective modes allow distinguishing diffusive modes, responsible for radiation trapping, from subradiant modes.

DOI: 10.1103/PhysRevA.95.053865

I. INTRODUCTION

Collective effects in light scattering by atomic ensembles are at the focus of intense research, both theoretically and experimentally [1]. Recently, the question of light localization in atomic media has been the subject of several studies based on an effective Hamiltonian approach [2–9]. From a total Hamiltonian describing a system of N atoms with at most one quantum of excitation (one photon), the degrees of freedom of the light field are traced over to get an effective non-Hermitian atomic Hamiltonian H_{eff}. In this approach, the eigenmodes and eigenvalues of H_{eff} are computed and analyzed. However, these quantities are not direct experimental observables, which makes the interpretation more difficult, in particular because the way the initial excitation entered the system is not specified. In a real experiment, the system is driven or excited by some external field and the outcome of the experiment depends on the parameters of this field.

Another, complementary approach has been used recently in the context of single-photon superradiance [10–13]: coupled-dipole equations (CDEs) [14,15]. This approach is based on the same effective Hamiltonian, but adding an external driving field is straightforward [16–18]. This describes the dynamics of the system in the low-intensity regime of excitation (linear optics) and allows computing experimental observables, such as the emission diagram [16,17], collective line shape and width [19–25], or the temporal dynamics of the scattered light [12,13,26–28].

The coupled-dipole equations including the external drive read

$$\dot{\beta}_i = \left(i\Delta - \frac{\Gamma_0}{2}\right)\beta_i - \frac{i\Omega(\boldsymbol{r})}{2} + \frac{i\Gamma_0}{2}\sum_{i\neq j} V_{ij}(r_{ij})\beta_j \ , \quad (1)$$

where β_i is the amplitude of the single-excited-atom state $|i\rangle = |g\cdots e_i\cdots g\rangle$ with $|g\rangle$ ($|e\rangle$) denoting the ground (excited) state, Δ is the detuning of the driving field from the two-level atomic dipolar transition, $\Omega(\boldsymbol{r}) = -dE(\boldsymbol{r})/\hbar$ its complex Rabi frequency with $E(\boldsymbol{r})$ the driving electric field, Γ_0 the natural decay rate for a single excited atoms, and $V_{ij}(r_{ij})$ is the dipole-dipole interaction (DDI) between atoms i and j, which depends on their separation r_{ij}. For simplicity we will consider only the scalar model of the DDI, which is relevant at low density. We will also set $\Gamma_0 = 1$ and drop it in the following. The first term of Eq. (1) corresponds to the natural evolution of the dipoles (oscillation and damping), the second one to the driving by the external laser, and the last term corresponds to the DDI interaction.

In the CDEs, the detuning Δ of the driving field is taken into account, but all collective effects [1]—the trivial ones like the refractive index and the beam attenuation, as well as the nontrivial ones like multiple scattering and super- and subradiance—come from the DDI term, in which the detuning does not directly enter. Since many collective effects obviously depend on the detuning, this can seem puzzling. Moreover, the long-lived modes discussed in the effective Hamiltonian approach [5–8] may be given different interpretations depending on the detuning (e.g., radiation trapping near resonance [29], or subradiance far from resonance [27]), although the eigenmodes themselves do not depend on the detuning. Understanding the influence of the detuning is thus crucial to making the link between the CDE and the effective Hamiltonian approach.

In this paper, we study the influence of the detuning on the *populations* of the collective modes, a quantity that has been overlooked so far, except in very few works [30,31]. In Sec. II we derive a simple and intuitive analytical expression relating the steady-state mode populations and the detuning. Although the result [Eq. (9)] is well known, we show in Sec. III that it has interesting and nonobvious consequences. In

*william.guerin@inphyni.cnrs.fr

particular, it allows us to understand why cooperative effects such as super- and subradiance become independent of the detuning at large detuning and why superradiance vanishes near resonance but not subradiance. Those behaviors are not intuitive and have already been observed experimentally and numerically [12,26,27]. We also show that subradiance and radiation trapping [29] can be attributed to collective modes with different eigenvalues, an interpretation supported by an analysis of the spatial properties of the corresponding eigenmodes. Finally, in Sec. IV, we present a numerical analysis of the weighted average of the eigenvalues, which puts in evidence empirical scaling laws.

II. ANALYTICAL RESULT

Let us first write the CDEs [Eq. (1)] in a matrix form,

$$\dot{\mathbf{B}} = \mathbf{M} \times \mathbf{B} + \mathbf{\Omega} \,, \tag{2}$$

with $\mathbf{B} = [\beta_1, \ldots, \beta_i, \ldots, \beta_N]^\intercal$, $\mathbf{\Omega} = -i/2 \times [\Omega(\boldsymbol{r_1}), \ldots, \Omega(\boldsymbol{r_i}), \ldots, \Omega(\boldsymbol{r_N})]^\intercal$, and

$$\mathbf{M} = \begin{bmatrix} -1/2 + i\,\Delta & \ldots & V_{1,N} \\ V_{2,1} & \ldots & V_{2,N} \\ \vdots & \ddots & \vdots \\ V_{N,1} & \ldots & -1/2 + i\,\Delta \end{bmatrix}. \tag{3}$$

We note that the detuning Δ appears as a constant shift of the imaginary part of the diagonal elements of the coupling matrix $\mathbf{M}$. As a consequence, it corresponds to a constant shift of all eigenfrequencies and does not change the eigenvectors. That is the reason why its influence is not discussed in the effective Hamiltonian approach [2–9], in which $H_{\text{eff}} = i\hbar\mathbf{M}(\Delta = 0)$ is used, although the correct definition of H_{eff} should in principle include the detuning [32].

By definition, the eigenvalues λ_k and eigenvectors $\mathbf{V}_k$ are such that $\mathbf{M} = \mathbf{V}\mathbf{D}\mathbf{V}^{-1}$ and $\mathbf{D} = \mathbf{V}^{-1}\mathbf{M}\mathbf{V}$, where $\mathbf{D} = \text{diag}(\lambda_1, \ldots, \lambda_k, \ldots, \lambda_N)$ and $\mathbf{V} = [\mathbf{V}_1, \ldots, \mathbf{V}_k, \ldots, \mathbf{V}_N]$.

Many experiments [12,27,29] consist of studying the dynamics of the system when it relaxes from the steady state to the ground state after the switch-off of the driving laser. This dynamics is then given by the natural evolution of each mode,

$$\mathbf{B}(t) = \sum_k \alpha_k \mathbf{V}_k e^{\lambda_k t} \,, \tag{4}$$

where the α_k are the complex coefficients of each mode, as given by the initial condition. In the case we consider here, the initial condition corresponds to the steady state reached when the driving laser is on. Let us call this steady state $\mathbf{B_0}$. Obviously,

$$\mathbf{B_0} = -\mathbf{M}^{-1}\mathbf{\Omega} = -(\mathbf{V}\mathbf{D}\mathbf{V}^{-1})^{-1}\mathbf{\Omega} = -\mathbf{V}\mathbf{D}^{-1}\mathbf{V}^{-1}\mathbf{\Omega} \,. \tag{5}$$

Let us also project the steady state $\mathbf{B_0}$ on the eigenmodes of the system, we have

$$\mathbf{B_0} = \sum_k \alpha_k \mathbf{V}_k \,, \tag{6}$$

where the coefficients of the decomposition are

$$\boldsymbol{\alpha} = [\alpha_1, \ldots, \alpha_k, \ldots, \alpha_N]^\intercal = \mathbf{V}^{-1}\mathbf{B_0} \,. \tag{7}$$

Using the expression (5) above for $\mathbf{B_0}$, $\boldsymbol{\alpha} = -\mathbf{D}^{-1}\mathbf{V}^{-1}\mathbf{\Omega}$, and we obtain, using the fact that $\mathbf{D}$ is diagonal,

$$\alpha_k = -\frac{(\mathbf{V}^{-1}\mathbf{\Omega})_k}{\lambda_k} = -\frac{P_k(\mathbf{\Omega})}{\lambda_k}, \tag{8}$$

where we note $P_k(\mathbf{\Omega})$ the kth coefficient of the decomposition of $\mathbf{\Omega}$ onto the basis made of all $\mathbf{V}_k$.

This relation is interesting because the weight of each eigenmode in the steady state appears as the product of two factors, one purely "geometrical," $\mathbf{V}^{-1}\mathbf{\Omega}$, which is the projection of the driving field on the eigenmodes, independent of the detuning, and one purely "spectral," the inverse of the corresponding eigenvalue, which does depend on the detuning. Defining the "population" $p_k = |\alpha_k|^2$ of the modes, and noting $\lambda_k = -\Gamma_k/2 + i\,E_k$, we have

$$p_k = \frac{|P_k(\mathbf{\Omega})|^2}{\Gamma_k^2/4 + \left(E_k^0 + \Delta\right)^2}, \tag{9}$$

where E_k^0 is the eigenfrequency for $\Delta = 0$ as in the H_{eff} approach. We recover an intuitive result, which describes a Lorentzian coupling efficiency to each mode. This Lorentzian depends on the width of the modes Γ_k and is shifted by the detuning Δ.

Note that this derivation and the result of Eqs. (8) and (9) is a simple example of the more general relations that exist between the effective Hamiltonian, its related scattering matrix, and decay rates, which are well known in the context of open quantum systems [see the reviews [32–35] and, for instance, Eq. (44) of [32]]. The similarities between cooperative scattering and the physics of open quantum systems has started to be discussed only recently [36,37]. Here, we just aim at discussing the consequences of this result on the decay of the steady state after the driving laser is switched off, and in particular the role of the initial detuning of the laser.

III. QUALITATIVE ANALYSIS

To fully understand the consequences of this result, let us turn to some graphical representations, where we plot the eigenvalue distribution of the coupling matrix in the complex plane. The main consequence of Eq. (9) is that the spectral factor $1/|\lambda_k|^2$ favors the modes located near the origin $E_k = \Gamma_k = 0$.

In the following, for simplicity, we will focus on the dilute limit, we thus do not discuss the localization problem [2–9], and we discard the near-field terms of the DDI, which are negligible in this limit. Our investigation is thus relevant, for example, to discuss the difference between subradiance [27] and radiation trapping [29], or the suppression of superradiance near resonance, as observed in a recent experiment [12].

In this dilute limit the DDI term is

$$V_{ij}(r_{ij}) = \frac{e^{ikr_{ij}}}{kr_{ij}}, \quad r_{ij} = |\boldsymbol{r}_i - \boldsymbol{r}_j|, \tag{10}$$

where $k = 2\pi/\lambda$ is the wave vector of the associated atomic transition.

Still for simplicity, we will also take the electric field $E(\boldsymbol{r})$ as a plane wave such that

$$\boldsymbol{\Omega} = -\frac{i\Omega}{2}[e^{ikz_1}, \ldots, e^{ikz_i}, \ldots, e^{ikz_N}]^{\intercal}. \tag{11}$$

We draw N random positions for the atoms in a spherical Gaussian distribution (rms width R) such that the density varies smoothly, thus avoiding sharp edges responsible for internal reflection of light [38,39]. We also apply an exclusion volume $kr_{ij} > 3$ to avoid pairs of very close atoms responsible for subradiant and superradiant branches in the complex plane [3,6,40,41]. These two phenomena are interesting in themselves but complicate the interpretation, because they can produce long-lived modes that are related to neither the collective N-body subradiance nor the diffusion of light. Then we diagonalize the coupling matrix $\mathbf{M}$ and compute the weight of the different modes using Eq. (9).

A. Influence of detuning

We show in Figs. 1 and 2 the outcome of such a computation, in which each panel shows the eigenvalue distribution in the complex plane for a single realization of the positions. Similar distributions have been studied before [2–9,40]. It is known that the eigenvalue distribution spreads from the single-atom limit $\{E_k = \Delta, \Gamma_k = 1\}$ as the on-resonance optical thickness $b_0 = 2N/(k_0R)^2$ increases, first forming a disk of radius $\propto\sqrt{b_0}$ for $b_0 \ll 1$, and then deforms at high b_0 with an accumulation of eigenvalues at small $\Gamma_k \ll 1$ and a corresponding spreading at high $\Gamma_k > 1$ [40]. This departure from single-atom physics exists at low density and is responsible for many collective effects in light scattering [1].

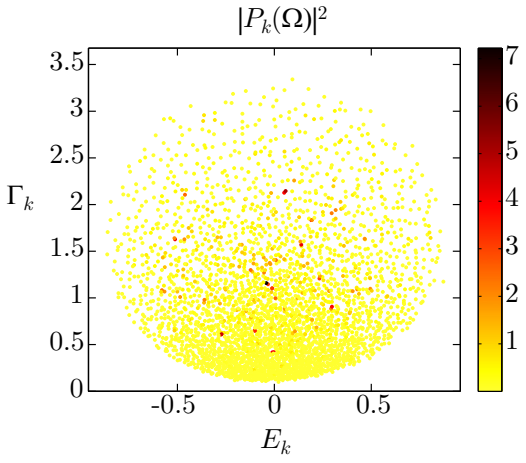

FIG. 1. Distribution of the eigenvalues $\lambda_k = -\Gamma_k/2 + iE_k$ in the complex plane (for $\Delta = 0$) with the geometrical factor $|P_k(\boldsymbol{\Omega})|^2$ represented in the color scale. The parameters of the atomic sample are $N = 3000$ and $kR \simeq 26.3$, yielding $b_0 \simeq 8.7$ and $\rho_0 k^{-3} \simeq 10^{-2}$.

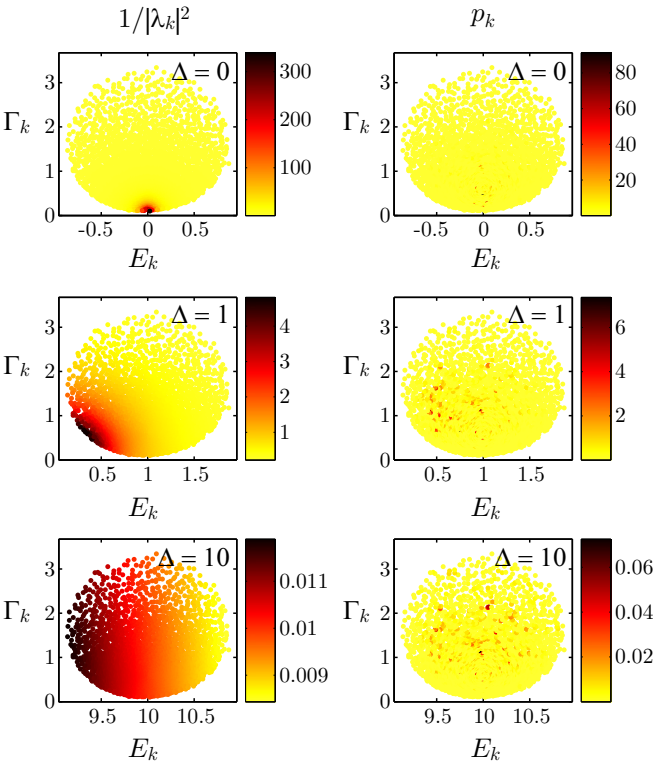

FIG. 2. Same as in Fig. 1 but the color scale now shows the spectral factor $1/|\lambda_k|^2$ (left column) and the populations p_k (right column). The different rows are for different detunings, from top to bottom $\Delta = 0, 1, 10$. Note the different color scale for each panel, showing that at large detuning, the spectral factor is almost uniform.

Here, we also show the geometrical factor $|P_k(\boldsymbol{\Omega})|^2$ (Fig. 1), the spectral factor $1/|\lambda_k|^2$ (Fig. 2, left column), and the population of the modes p_k (Fig. 2, right column) encoded in the color scale. The different rows of Fig. 2 are for different detunings, on resonance $\Delta = 0$ (first row), slightly detuned $\Delta = 1$ (second row), and far detuned $\Delta = 10$ (third row). The geometrical factor (Fig. 1) does not depend on the detuning. Here we have chosen a moderately large on-resonance optical thickness $b_0 \simeq 9$ and a low density $\rho_0 k^{-3} \simeq 10^{-2}$ (ρ_0 is the peak atomic density). Since the problem is linear, the value of Ω can be chosen at will and we have taken $\Omega = 2/\sqrt{N}$ such that $\boldsymbol{\Omega}$ is normalized to unity.

From these figures, several relevant observations can be made: (1) Only a few modes, mainly selected by the geometrical factor, have a non-negligible population and thus contribute to the dynamics of the system. Studying the whole eigenvalue distribution is thus not directly relevant to the experiment. In particular, the extreme modes, for example, the most superradiant ones, whose eigenvalues lie on the border of the distribution, are not significantly populated. (2) The geometrical factor favors the short-lived modes, i.e., the superradiant modes ($\Gamma_k > 1$). This was expected from the idea that superradiant modes are more coupled to the environment than subradiant modes. (3) Far from resonance, the spectral factor only induces an overall decrease of the populations and has a negligible effect on the mode selection. (4) It is very hard, if not impossible, to select any specific

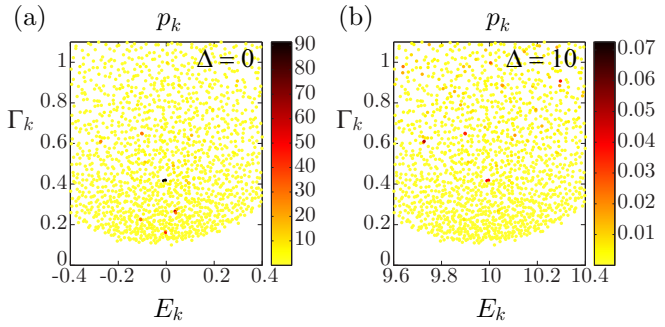

FIG. 3. Close-up of the populations of the long-lived modes, at resonance (a) and far from resonance (b). Same parameters as in Fig. 1.

mode by tuning the driving field frequency. For the $\Delta = 1$ case, for example, one might expect to selectively populate modes on the left border of the distribution, but that is actually not the case. The geometrical factor dominates over the spectral factor. Other strategies, based for instance on the spatial shaping of the driving field, are needed to selectively populate targeted modes [42]. (5) The spectral factor has an important effect only near resonance. It strongly favors the long-lived modes and thus decreases considerably the relative population of the superradiant modes. This demonstrates that superradiance disappears near resonance, as observed in previous experiments and numerical simulations [12,43].

A closer look on the populations of the long-lived modes is shown in Fig. 3(a) for the resonant case and in Fig. 3(b) for the far-detuned case. Even on resonance, only a few modes are strongly populated, showing that the geometrical factor still plays an important role. At large detuning, the long-lived modes that are populated are responsible for subradiance. These modes are still populated (and even more) near resonance, showing that the relative weight of subradiance increases near resonance, as seen experimentally [27]. Moreover, in addition to the modes strongly populated at large detuning, additional eigenmodes acquire noticeable population near resonance, with even longer lifetimes. These modes are responsible for radiation trapping due to multiple scattering [29]. This interpretation is validated by an analysis of the spatial properties of the modes, summarized in Fig. 4 and detailed in the next section.

At large detuning, the effect of the spectral factor on the relative population of the eigenmodes is negligible and completely vanishes for $\Delta \to \infty$, such that the relative populations are only given by the geometrical factor $|P_k(\mathbf{\Omega})|^2$, which actually means that the steady state $\mathbf{B_0}$ is proportional to $\mathbf{\Omega}$. This is precisely the timed-Dicke (TD) state approximation, introduced for single-photon excitation by Scully *et al.* [10] and further developed for continuous driving in Refs. [16–18]. Although this state is mainly superradiant, even though not the largest Γ_k of the distribution, it also contains subradiant components [Fig. 3(b)], as recently observed experimentally [27]. In other words, using a large detuning causes the driving field to couple weakly, but *equally*, to all modes having a good geometrical overlap with the driving field, and it thus reveals a part of the underlying mode structure, which is independent of the detuning. The consequence is that the collective dynamics after switching off the driving field is still cooperative at very large detuning, with superradiant and subradiant decay rates becoming asymptotically independent of the detuning.

B. Spatial properties of the modes

It is also interesting to study the spatial properties of the collective modes in order to identify their physical meaning. Two quantities are useful to characterize the mode spatial properties: the rms size of the modes σ_k and the participation ratio (PR), defined as

$$\mathcal{R}_k^{\mathrm{P}} = \frac{\sum_i |V_{ki}|^2}{\sum_i |V_{ki}|^4}\ , \tag{12}$$

which indicates the number of atoms participating significantly to the mode [5,44]. We represent in Figs. 4(a) and 4(b) these two quantities in the color scale of the eigenvalue distribution. We observe three distinctive areas: (i) Near the single-atom-physics case $\{E_k = 0, \Gamma_k = 1\}$, the modes have a larger rms size than the Gaussian atomic sample, $\sigma_k > R$, and a local minimum of the PR. This denotes modes delocalized at the boundary of the sample. Physically, this situation corresponds to single scattering (or low-order scattering) on the edges of the sample, as confirmed by the profile shown in Fig. 4(c). (ii) For the longest-lived modes ($\Gamma_k \ll 1$, at the border of the distribution), the size and the PR are both small, which means that the modes are not very extended. As seen in Fig. 4(d), they are located at the center of the sample. We attribute this behavior to diffusive modes due to multiple scattering. (iii) In the rest of the complex plane (most modes), the modes have approximately the same size as the

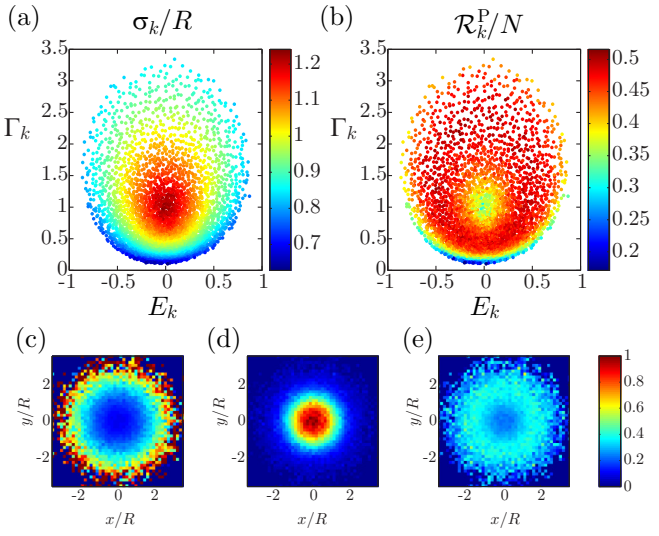

FIG. 4. Spatial properties of the collective modes. Same parameters are in Fig. 1, but the color scale now shows (a) the rms size σ_k of the modes (normalized by the sample size R), and (b) the participation ratio $\mathcal{R}_k^{\mathrm{P}}$ (normalized by the atom number N). We show in panels (c)–(e) the average over 120 realizations of the excitation probability (mode intensity divided by atomic density) for atoms located in a slice $|z| < R/5$, for each kind of mode, selected by the following conditions: (c) $0.9 < \Gamma_k < 1.1$ and $-0.1 < E_k < 0.1$; (d) $\Gamma_k < 0.2$; (e) $PR_k > 0.45$.

sample ($\sigma_k \sim R$) and a maximum PR (around $N/2$). They correspond to collective and extended modes, with almost uniform excitation probability across the sample Fig. 4(e). These modes can exhibit superradiant ($\Gamma_k > 1$) or subradiant ($\Gamma_k < 1$ or $\Gamma_k \ll 1$) behavior.

This analysis validates the interpretation given above on the different nature of the long-lived modes that are populated near resonance (diffusive modes responsible for radiation trapping [29]) compared to those excited far from resonance (subradiant modes).

IV. NUMERICAL STUDY

Many statistical quantities can in principle be computed and studied from the eigenvalue distribution [2–9,40]. Here we will focus on quantities that use the information contained in the populations p_k. These quantities, not studied before, are thus not only related to the properties of the effective Hamiltonian, but also to the way the system is excited. In particular, they will depend on the detuning Δ. They are thus less universal, but they are more related to experimental observables. One can thus expect to recover qualitative behaviors similar to what has been observed in experiments or in numerical simulations of the CDEs.

A. Behavior of the weighted averages

Let us now turn to a systematic analysis of the weighted averages of the eigenfrequencies (or eigenenergies) and decay rates (or linewidth), defined as

$$\langle E\rangle = \frac{\sum_k p_k E_k}{\sum_k p_k} \quad \text{and} \quad \langle\Gamma\rangle = \frac{\sum_k p_k \Gamma_k}{\sum_k p_k}. \tag{13}$$

We show in Fig. 5 a systematic study of these quantities as a function of the on-resonance optical thickness b_0 and on the detuning Δ. For each b_0, 120 realizations of the disorder configuration have been used.

We observe that the average eigenenergy is slightly shifted from Δ and the shift $\langle E\rangle - \Delta$ displays a dispersion-like behavior, which becomes higher and broader as the optical thickness increases. On the contrary, the average decay rate $\langle\Gamma\rangle$ exhibits a negative resonance-like structure, which is also more important at larger b_0. These behaviors are due to the spectral factor and can be qualitatively understood as follows.

First, on resonance ($\Delta = 0$), positive and negative values of E_k compensate so that $\langle E\rangle = 0$ after averaging over the disorder configurations (we remain here in the dilute limit such that the cooperative Lamb shift is negligible [20–24,45–51]). The same applies at very large detuning, for which the spectral factor plays a negligible role on the relative populations. At intermediate detuning, the spectral factor favors one side of the eigenvalue distribution, such that $\langle E\rangle$ departs from Δ to get slightly closer to zero [Fig. 2]. The difference $\langle E\rangle - \Delta$ has thus an opposite sign from Δ, which produces a dispersion behavior for the frequency shift, similar to an effective refractive index. This effect is more important as the eigenvalue distribution spreads for increasing b_0.

Similarly for $\langle\Gamma\rangle$, at large detuning, the geometrical factor dominates and we have seen previously that it favors the superradiant modes, such that $\langle\Gamma\rangle > 1$, and superradiance is stronger as b_0 increases. We can actually compute $\langle\Gamma\rangle$ in the $\Delta \to \infty$ limit (TD approximation) by replacing the populations by the geometrical factor in the averaging Eq. (13). We clearly observe in Fig. 5(c) a linear scaling with b_0:

$$\langle\Gamma\rangle_{\Delta\to\infty} = 1 + \frac{b_0}{24}. \tag{14}$$

We note that a similar linear scaling is expected for the superradiant decay rate of the TD state [12,13,16,52–56].

On resonance, however, the spectral factor favors the long-lived modes [Fig. 2] and thus $\langle\Gamma\rangle$ drops to values smaller than unity. Interestingly, we have found [Fig. 5(c)] that the data follow very closely the empirical relationship

$$\langle\Gamma\rangle_{\Delta=0} = 1 - \tfrac{1}{4}(1 - e^{-b_0/8}), \tag{15}$$

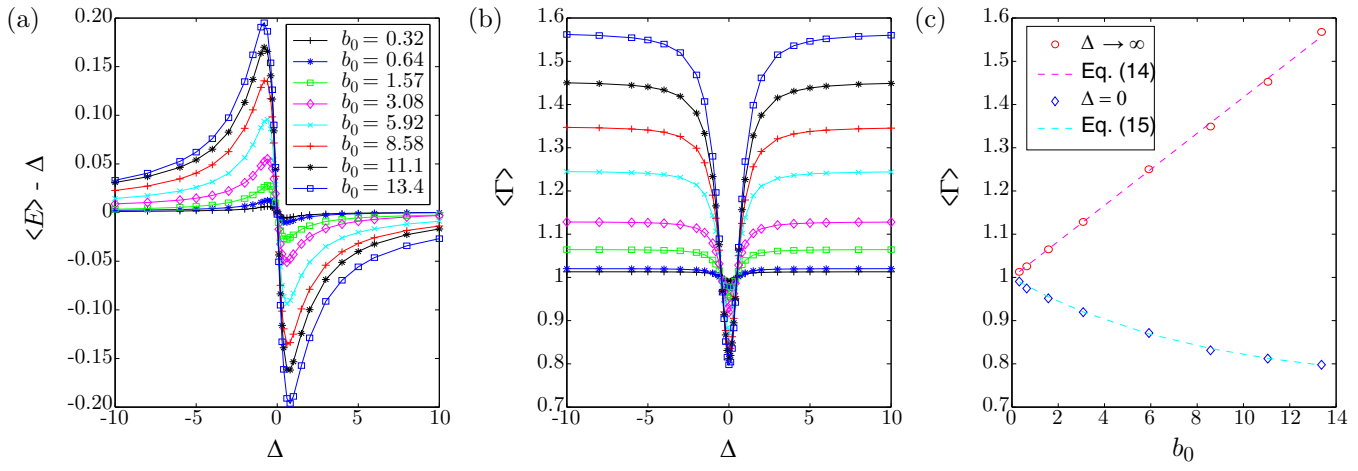

FIG. 5. Study of the weighted averages $\langle E\rangle$ and $\langle\Gamma\rangle$ [Eq. (13)] as a function of the detuning Δ and the on-resonance optical thickness b_0. (a) The frequency shift $\langle E\rangle - \Delta$ is plotted as a function of Δ for different b_0. (b) $\langle\Gamma\rangle$ is plotted as a function of Δ for different b_0. (c) $\langle\Gamma\rangle$ is plotted as a function of b_0 for the two extreme cases, $\Delta \to \infty$ (red circles) and $\Delta = 0$ (blue diamonds). The dashed lines correspond to the empirical relations given in Eqs. (14) and (15).

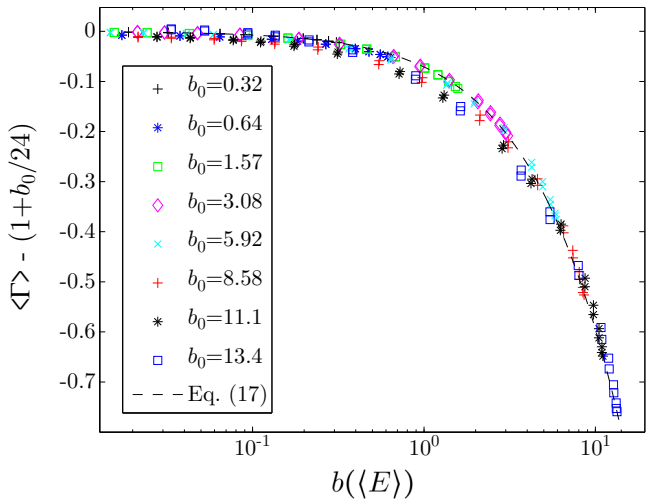

FIG. 6. Same numerical data as in Figs. 5(a) and 5(b) but $\langle\Gamma\rangle - (1 + b_0/4)$ is plotted as a function of $b(\langle E\rangle) = b_0/(1 + 4\langle E\rangle^2)$ (log scale). All points collapse on a single curve (dashed line), well described by Eq. (17) .

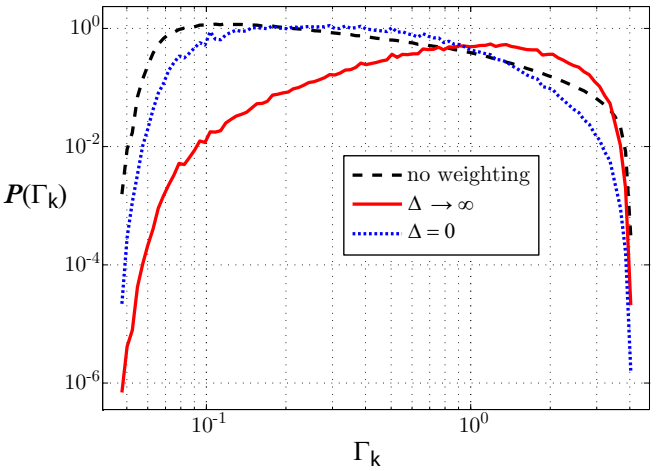

FIG. 7. Linewidth distribution $P(\Gamma_k)$ without weighting (dashed black line) and with weighting corresponding to the populations p_k computed far from resonance ($\Delta \to \infty$, solid red line) or at resonance ($\Delta = 0$, dotted blue line). The parameters of the atomic sample are $N = 5000$, $kR \simeq 27.3$ yielding $b_0 \simeq 13.4$, $\rho_0 k^{-3} \simeq 1.55 \times 10^{-2}$, and we used 120 realizations.

which denotes an exponential decrease of $\langle\Gamma\rangle$ with the optical thickness, with a saturation effect. This is consistent with the idea that attenuation and multiple scattering suppress superradiance, as observed in Ref. [12] and in Fig. 2, but the plane-wave illumination ensures that there is always a large proportion of single scattering at the borders of the atomic cloud, and thus a large fraction of modes with $\Gamma_k \sim 1$, such that $\langle\Gamma\rangle_{\Delta=0}$ does not decrease to zero as b_0 increases.

Given the relatively simple behaviors of $\langle\Gamma\rangle$ and $\langle E\rangle$, one can wonder whether a more general relationship between $\langle\Gamma\rangle$, $\langle E\rangle$, and b_0 can be found. The limit cases [Eqs. (14) and (15)] suggest a route to a more refined scaling law. Plotting $\langle\Gamma\rangle - (1 + b_0/24)$ as a function of the detuning Δ exhibits a Lorentzian absorption profile whose depth and width depends on b_0. It is thus natural to plot it as a function of $b(\Delta) = b_0/(1 + 4\Delta^2)$. The points then tend to collapse on a single curve, but with significant deviations. In fact, $b(\Delta)$ would be the actual optical thickness at the laser detuning without cooperativity. To take into account the spreading of the eigenvalue distribution, it makes sense to replace $b(\Delta)$ by

$$b(\langle E\rangle) = \frac{b_0}{1 + 4\langle E\rangle^2}\,. \tag{16}$$

In that case, all data points collapse almost perfectly on a single curve (Fig. 6). This curve is well described by

$$\langle\Gamma\rangle - \left(1 + \frac{b_0}{24}\right) \simeq -\frac{b(\langle E\rangle)}{24} - \frac{1}{4}(1 - e^{-b(\langle E\rangle)/8}), \tag{17}$$

or, in a more compact form, defining $b \equiv b(\langle E\rangle)$,

$$\langle\Gamma\rangle \simeq 1 + \frac{1}{4}\left[\frac{b_0 - b}{6} - (1 - e^{-b/8})\right], \tag{18}$$

which contains the previous limiting cases. The quality of the collapse on such a universal curve as seen in Fig. 6 and expressed by Eq. (18) suggests that it should be possible to obtain analytical results describing the observed behaviors.

B. Linewidth distribution

Another interesting quantity is the distribution of the linewidths, $P(\Gamma_k)$. This distribution has been studied in several papers [4,6,57,58], but here we include p_k as a weighting factor of the Γ_k in the distribution $P(\Gamma_k)$, still computed over 120 realizations of the positions.

We show in Fig. 7 the comparison of the distribution $P(\Gamma_k)$ without weighting (and thus independent of Δ), with the ones computed with weighting corresponding to $\Delta \to \infty$ and $\Delta = 0$ (and excitation by a plane wave, as previously). As expected from the previous discussions, taking into account the weighting due to the population p_k increases the probability density of the short-lived (superradiant) modes far from resonance and of the long-lived modes near resonance. We note that this distribution $P(\Gamma_k)$ has a strong dependance on the detuning. This suggests that a characterization of the transport properties of light through resonant two-level systems needs to go beyond a mere eigenvalues analysis [4], since the transport properties obviously depend on the detuning. In general, the distribution $P(\Gamma_k)$ depends on the way the system is coupled to the environment [33,58].

We also note that the linewidth distribution does not allow us to extract any specific value for the long-lived modes effectively populated by an external drive, even when taking into account the weighting function of Eq. (9). Therefore, we cannot recover the scaling laws that can be observed in experiments on subradiance [27] or radiation trapping [29], indicating that the approach presented in this paper is not sufficient to recover experimentally observed scaling laws.

C. Discussion

We attribute this limitation to the fact that the quantities studied in this paper (such as the Γ_k) are not direct experimental observables. Indeed, when measuring the light escaping from

the atomic sample, for example, the total scattered power [41]

$$P \propto -\frac{d}{dt}\sum_{i=1}^{N}|\beta_i(t)|^2 = -\frac{d}{dt}\|\mathbf{B}(t)\| = -\frac{d}{dt}\left\|\sum_k \alpha_k \mathbf{V}_k e^{\lambda_k t}\right\|, \quad (19)$$

the nonorthogonality of the eigenmodes $\mathbf{V}_k$ (due to the non-Hermiticity of the effective Hamiltonian) are at the origin of oscillating terms [34], which may change the dynamics of the decay, even after configuration averaging. It is thus not surprising to find a quantitative difference in the decay rates. For example, the linear scaling of $\langle\Gamma\rangle$ with b_0 obtained at Eq. (14) does not have the same slope as what has been found by studying the decay of the scattered light in the coupled-dipole model [12,41]. Obtaining analytical results on experimental observables remains thus an open problem.

In the framework of the effective Hamiltonian approach, one can also study the spectrum of the Hermitian operator $\mathrm{Im}(H_{\mathrm{eff}})$ [59]. In that case, the eigenvalues are directly related to the probability of returning in the ground state, and thus correspond to the light escape rates from the sample [60,61]. However, this is only valid when the initial state contains one excitation but no coherence, and thus does not apply to driven systems.

V. CONCLUSION

Several properties of cooperative scattering, such as the enhancement of subradiance and suppression of superradiance near resonance [12,27], and the very existence of cooperative decay at very large detuning, are highly nonintuitive. We have shown in this paper that they are consequences of the simple analytical relationship that exists between the population of the collective modes of the effective Hamiltonian and the detuning of the driving field [Eq. (9)]. We have also put in evidence an empirical scaling law on the weighted averages of the eigenvalues of the effective Hamiltonian, which suggests the possibility of further analytical results.

In general, statistical properties of the eigenvalues of the effective Hamiltonian can be efficiently studied using random matrix theory [40], whereas very few analytical results have been obtained from the coupled-dipole equation model [15,54]. The populations of the collective modes and their dependence on the parameters of the driving field is an important ingredient bridging the gap between the two approaches.

We also discussed the spatial properties of the modes and showed that we can distinguish two kinds of long-lived modes that can be associated with radiation trapping and subradiance. Extending this analysis to the high-density case could be useful to better understand the transition to Anderson localization [5,6].

ACKNOWLEDGMENTS

We thank Johannes Schachenmayer for careful reading of the manuscript. We acknowledge financial support from the ANR (Agence National pour la Recherche, project LOVE, No. ANR-14-CE26-0032).

[1] W. Guerin, M. T. Rouabah, and R. Kaiser, Light interacting with atomic ensembles: Collective, cooperative and mesoscopic effects, J. Mod. Opt. **64**, 895 (2017).

[2] M. Rusek, A. Orłowski, and J. Mostowski, Localization of light in three-dimensional random dielectric media, Phys. Rev. E **53**, 4122 (1996).

[3] M. Rusek, J. Mostowski, and A. Orłowski, Random green matrices: From proximity resonances to Anderson localization, Phys. Rev. A **61**, 022704 (2000).

[4] F. A. Pinheiro, M. Rusek, A. Orlowski, and B. A. van Tiggelen, Probing Anderson localization of light via decay rate statistics, Phys. Rev. E **69**, 026605 (2004).

[5] S. E. Skipetrov and I. M. Sokolov, Absence of Anderson Localization of Light in a Random Ensemble of Point Scatterers, Phys. Rev. Lett. **112**, 023905 (2014).

[6] L. Bellando, A. Gero, E. Akkermans, and R. Kaiser, Cooperative effects and disorder: A scaling analysis of the spectrum of the effective atomic Hamiltonian, Phys. Rev. A **90**, 063822 (2014).

[7] S. E. Skipetrov and I. M. Sokolov, Magnetic-Field-Driven Localization of Light in a Cold-Atom Gas, Phys. Rev. Lett. **114**, 053902 (2015).

[8] C. E. Máximo, N. Piovella, P. W. Courteille, R. Kaiser, and R. Bachelard, Spatial and temporal localization of light in two dimensions, Phys. Rev. A **92**, 062702 (2015).

[9] S. E. Skipetrov, Finite-size scaling analysis of localization transition for scalar waves in a three-dimensional ensemble of resonant point scatterers, Phys. Rev. B **94**, 064202 (2016).

[10] M. O. Scully, E. S. Fry, C. H. R. Ooi, and K. Wódkiewicz, Directed Spontaneous Emission from an Extended Ensemble of N Atoms: Timing is Everything, Phys. Rev. Lett. **96**, 010501 (2006).

[11] M. O. Scully and A. A. Svidzinsky, The super of superradiance, Science **325**, 1510 (2009).

[12] M. O. Araújo, I. Krešić, R. Kaiser, and W. Guerin, Superradiance in a Large Cloud of Cold Atoms in the Linear-Optics Regime, Phys. Rev. Lett. **117**, 073002 (2016).

[13] S. J. Roof, K. J. Kemp, M. D. Havey, and I. M. Sokolov, Observation of Single-Photon Superradiance and the Cooperative Lamb Shift in an Extended Sample of Cold Atoms, Phys. Rev. Lett. **117**, 073003 (2016).

[14] J. Javanainen, J. Ruostekoski, B. Vestergaard, and M. R. Francis, One-dimensional modeling of light propagation in dense and degenerate samples, Phys. Rev. A **59**, 649 (1999).

[15] A. A. Svidzinsky, J.-T. Chang, and M. O. Scully, Cooperative spontaneous emission of N atoms: Many-body eigenstates, the effect of virtual Lamb shift processes, and analogy with radiation of N classical oscillators, Phys. Rev. A **81**, 053821 (2010).

[16] Ph. W. Courteille, S. Bux, E. Lucioni, K. Lauber, T. Bienaimé, R. Kaiser, and N. Piovella, Modification of radiation pressure

due to cooperative scattering of light, Eur. Phys. J. D. **58**, 69 (2010).
[17] T. Bienaimé, M. Petruzzo, D. Bigerni, N. Piovella, and R. Kaiser, Atom and photon measurement in cooperative scattering by cold atoms, J. Mod. Opt. **58**, 1942 (2011).
[18] T. Bienaimé, R. Bachelard, P. W. Courteille, N. Piovella, and R. Kaiser, Cooperativity in light scattering by cold atoms, Fortschr. Phys. **61**, 377 (2013).
[19] L. Chomaz, L. Corman, T. Yefsah, R. Desbuquois, and J. Dalibard, Absorption imaging of a quasi-two-dimensional gas: A multiple scattering analysis, New J. Phys. **14**, 055001 (2012).
[20] J. Javanainen, J. Ruostekoski, Y. Li, and S.-M. Yoo, Shifts of a Resonance Line in a Dense Atomic Sample, Phys. Rev. Lett. **112**, 113603 (2014).
[21] Z. Meir, O. Schwartz, E. Shahmoon, D. Oron, and R. Ozeri, Cooperative Lamb Shift in a Mesoscopic Atomic Array, Phys. Rev. Lett. **113**, 193002 (2014).
[22] S. L. Bromley, B. Zhu, M. Bishof, X. Zhang, T. Bothwell, J. Schachenmayer, T. L. Nicholson, R. Kaiser, S. F. Yelin, M. D. Lukin, A. M. Rey, and J. Ye, Collective atomic scattering and motional effects in a dense coherent medium, Nat. Commun. **7**, 11039 (2016).
[23] S. Jennewein, M. Besbes, N. J. Schilder, S. D. Jenkins, C. Sauvan, J. Ruostekoski, J.-J. Greffet, Y. R. P. Sortais, and A. Browaeys, Coherent Scattering of Near-Resonant Light by a Dense Microscopic Cold Atomic Cloud, Phys. Rev. Lett. **116**, 233601 (2016).
[24] B. Zhu, J. Cooper, J. Ye, and A. M. Rey, Light scattering from dense cold atomic media, Phys. Rev. A **94**, 023612 (2016).
[25] R. T. Sutherland and F. Robicheaux, Coherent forward broadening in cold atom clouds, Phys. Rev. A **93**, 023407 (2016).
[26] T. Bienaimé, N. Piovella, and R. Kaiser, Controlled Dicke Subradiance from a Large Cloud of two-Level Systems, Phys. Rev. Lett. **108**, 123602 (2012).
[27] W. Guerin, M. O. Araújo, and R. Kaiser, Subradiance in a Large Cloud of Cold Atoms, Phys. Rev. Lett. **116**, 083601 (2016).
[28] S. E. Skipetrov, I. M. Sokolov, and M. D. Havey, Control of light trapping in a large atomic system by a static magnetic field, Phys. Rev. A **94**, 013825 (2016).
[29] G. Labeyrie, E. Vaujour, C. A. Müller, D. Delande, C. Miniatura, D. Wilkowski, and R. Kaiser, Slow Diffusion of Light in a Cold Atomic Cloud, Phys. Rev. Lett. **91**, 223904 (2003).
[30] Y. Li, J. Evers, W. Feng, and S.-Y. Zhu, Spectrum of collective spontaneous emission beyond the rotating-wave approximation, Phys. Rev. A **87**, 053837 (2013).
[31] W. Feng, Y. Li, and S.-Y. Zhu, Effect of atomic distribution on cooperative spontaneous emission, Phys. Rev. A **89**, 013816 (2014).
[32] I. Rotter, A non-Hermitian Hamilton operator and the physics of open quantum systems, J. Phys. A **42**, 153001 (2009).
[33] F.-M. Dittes, The decay of quantum systems with a small number of open channels, Phys. Rep. **339**, 215 (2000).
[34] J. Okołowicz, M. Płoszajczak, and I. Rotter, Dynamics of quantum systems embedded in a continuum, Phys. Rep. **374**, 271 (2003).
[35] U. Kuhl, O. Legrand, and F. Mortessagne, Microwave experiments using open chaotic cavities in the realm of the effective Hamiltonian formalism, Fortschr. Phys. **61**, 404 (2012).
[36] *Special Issue: Quantum Physics with non-Hermitian Operators: Theory and Experiment*, edited by J. P. Bird, R. Kaiser, I. Rotter, and G. Wunner, Fortschr. Phys., Vol. 61 (Wiley, Weinheim, 2012).
[37] I. Rotter and J. P. Bird, A review of progress in the physics of open quantum systems: Theory and experiment, Rep. Prog. Phys. **78**, 114001 (2015).
[38] R. Bachelard, P. W. Courteille, R. Kaiser, and N. Piovella, Resonances in Mie scattering by an inhomogeneous atomic cloud, Europhys. Lett. **97**, 14004 (2012).
[39] N. J. Schilder, C. Sauvan, J.-P. Hugonin, S. Jennewein, Y. R. P. Sortais, A. Browaeys, and J.-J. Greffet, Role of polaritonic modes on light scattering from a dense cloud of atoms, Phys. Rev. A **93**, 063835 (2016).
[40] S. E. Skipetrov and A. Goetschy, Eigenvalue distributions of large Euclidean random matrices for waves in random media, J. Phys. A **44**, 065102 (2011).
[41] M. O. Araújo, W. Guerin, and R. Kaiser, Decay dynamics in the coupled-dipole model, arXiv:1705.02190.
[42] M. O. Scully, Single Photon Subradiance: Quantum Control of Spontaneous Emission and Ultrafast Readout, Phys. Rev. Lett. **115**, 243602 (2015).
[43] This discussion does not apply to experiments using a pulsed excitation, as in Ref. [13], since we are dealing with the steady state obtained with a continuous monochromatic excitation. For a detailed study about the influence of the exciting pulse duration, see A. S. Kuraptsev, I. Sokolov, and M. D. Havey, Angular distribution of single photon superradiance in a dilute and cold atomic ensemble, arXiv:1701.07503.
[44] A. Biella, F. Borgonovi, R. Kaiser, and G. L. Celardo, Subradiant hybrid states in the open 3D Anderson-Dicke model, Europhys. Lett. **103**, 57009 (2013).
[45] R. Friedberg, S. R. Hartmann, and J. T. Manassah, Frequency shifts in emission and absorption by resonant systems of two-level atoms, Phys. Rep. **7**, 101 (1973).
[46] M. O. Scully, Collective Lamb Shift in Single Photon Dicke Superradiance, Phys. Rev. Lett. **102**, 143601 (2009).
[47] R. Röhlsberger, K. Schlage, B. Sahoo, S. Couet, and R. Rüffer, Collective Lamb shift in single-photon superradiance, Science **328**, 1248 (2010).
[48] J. Keaveney, A. Sargsyan, U. Krohn, I. G. Hughes, D. Sarkisyan, and C. S. Adams, Cooperative Lamb Shift in an Atomic Vapor Layer of Nanometer Thickness, Phys. Rev. Lett. **108**, 173601 (2012).
[49] J. T. Manassah, Cooperative radiation from atoms in different geometries: Decay rate and frequency shift, Adv. Opt. Photon. **4**, 108 (2012).
[50] S. D. Jenkins, J. Ruostekoski, J. Javanainen, R. Bourgain, S. Jennewein, Y. R. P. Sortais, and A. Browaeys, Optical Resonance Shifts in the Fluorescence of Thermal and Cold Atomic Gases, Phys. Rev. Lett. **116**, 183601 (2016).
[51] J. Javanainen and J. Ruostekoski, Light propagation beyond the mean-field theory of standard optics, Opt. Express **24**, 993 (2016).
[52] I. E. Mazets and G. Kurizki, Multiatom cooperative emission following single-photon absorption: Dicke-state dynamics, J. Phys. B **40**, F105 (2007).

[53] A. A. Svidzinsky, J.-T. Chang, and M. O. Scully, Dynamical Evolution of Correlated Spontaneous Emission of a Single Photon from a Uniformly Excited Cloud of N Atoms, Phys. Rev. Lett. **100**, 160504 (2008).

[54] A. A. Svidzinsky and J.-T. Chang, Cooperative spontaneous emission as a many-body eigenvalue problem, Phys. Rev. A **77**, 043833 (2008).

[55] R. Friedberg and J. T. Manassah, Analytic expressions for the initial cooperative decay rate and cooperative Lamb shift for a spherical sample of two-level atoms, Phys. Lett. A **374**, 1648 (2010).

[56] S. Prasad and R. J. Glauber, Coherent radiation by a spherical medium of resonant atoms, Phys. Rev. A **82**, 063805 (2010).

[57] T. Kottos and M. Weiss, Statistics of Resonance and Delay Times: A Criterion for Metal-Insulator Transition, Phys. Rev. Lett. **89**, 056401 (2002).

[58] M. Weiss, J. A. Méndez-Bermúdez, and T. Kottos, Resonance width distribution for high-dimensional random media, Phys. Rev. B **73**, 045103 (2006).

[59] E. Akkermans, A. Gero, and R. Kaiser, Photon Localization and Dicke Superradiance in Atomic Gases, Phys. Rev. Lett. **101**, 103602 (2008).

[60] V. Ernst and P. Stehle, Emission of radiation from a system of many excited atoms, Phys. Rev. **176**, 1456 (1968).

[61] E. Ressayre and A. Tallet, Quantum theory for superradiance, Phys. Rev. A **15**, 2410 (1977).